Impact of surface functionalization on the uptake mechanism and toxicity effects of silver nanoparticles in HepG2 cells

Brkić Ahmed, Lada; Milić, Mirta; Pongrac, Igor M.; Marjanović, Ana Marija; Mlinarić, Hrvoje; Pavičić, Ivan; Gajović, Srećko; Vinković Vrček, Ivana

Brkić Ahmed L., Milić M., Pongrac I. M., Marjanović A. M., Mlinarić H., Pavičić I., Gajović S., Vinković Vrček I. (2017) ***Impact of surface functionalization on the uptake mechanism and toxicity effects of silver nanoparticles in HepG2 cells.*** **Food and Chemical Toxicology, 107 (Pt. A). pp. 349-61. ISSN 0278-6915**

http://www.elsevier.com/locate/issn/02786915

http://www.sciencedirect.com/science/journal/02786915

http://dx.doi.org/10.1016/j.fct.2017.07.016

Impact of surface functionalization on the uptake mechanism and toxicity effects of silver nanoparticles in HepG2 cells

Lada Brkić Ahmed[a], Mirta Milić[b], Igor M. Pongrac[a], Ana Marija Marjanović[b], Hrvoje Mlinarić[a], Ivan Pavičić[b], Srećko Gajović[a] and Ivana Vinković Vrček[b, *]

[a] University of Zagreb, School of Medicine, Croatian Institute for Brain Research, Šalata 12, 10 000 Zagreb, Croatia

[b] Institute for Medical Research and Occupational Health, Ksaverska cesta 2, 10 000 Zagreb, Croatia

RUNNING TITLE: Toxicity and uptake of silver nanoparticles in HepG2 cells

[*]Corresponding author: I. Vinković Vrček, Institute for Medical Research and Occupational Health, Ksaverska cesta 2, 10 000 Zagreb, Croatia; Tel: +385 1 4682540 E-mail: ivinkovic@imi.hr

Abstract

Safe and successful bioapplications of metallic nanoparticles depend on their physicochemical characteristics, in particular their surface properties. This study aimed to investigate how different surface functionalization of silver nanoparticles (AgNP) affect their interaction with mammalian liver cells with regard to cytotoxicity, genotoxicity and mechanism of cellular uptake. Differentially coated AgNP were prepared by surface functionalization using sodium bis(2-ethylhexyl)-sulfosuccinate (AOTAgNP), cetyltrimethylammonium bromide (CTABAgNP), poly(vinylpyrrolidone) (PVPAgNP), poly-L-lysine (PLLAgNP), and bovine serum albumin (BSAAgNP). Data showed varying toxic potential of differentially coated AgNP. All AgNP types demonstrated concentration dependent effects on cytotoxicity and genotoxicity in HepG2 cells. Cytotoxic potential of differentially coated AgNP followed the order of BSAAgNP > PLLAgNP > CTABAgNP > AOTAgNP > PVPAgNP. Exposure of HepG2 cells to non-cytotoxic concentrations (up to 10 mg Ag/L) of AgNP for 24 hr induced primary DNA damage as evaluated by alkaline comet assay. The highest increase in both comet tail length and tail intensity was produced by PLLAgNP followed by AOTAgNP, while CTABAgNP appeared to be least damaging. The main uptake mechanisms of AgNP were macropinocytosis and clathrin-mediated endocytosis. The study findings contribute to the criteria that should be considered in evaluating the biocompatibility and safety of novel nanomaterials.

***Key words*:** silver nanoparticles, surface functionalization, cytotoxicity, genotoxicity, cellular uptake, HepG2 cells

Funding

This work was supported by the GlowBrain project (FP7-REGPOT–2012–CT2012–316120; European Commission) and by the Croatian Science Foundation [grant number IP-2016-06-2436]

1. Introduction

Given the progressive applications of silver nanoparticles (AgNP) in medicine and general consumer products, comprehensive understanding of nanoparticles (NP) interaction with living organisms is imperative (Kermanizadeh et al., 2016). There is ever growing concern over health impacts of a wide range of AgNP in usage including burns treatment, textiles, water purification devices, toothbrushes, shampoo, deodorants, and food packaging materials (Bondarenko et al., 2013). Metallic NP are known to induce oxidative stress by disruption of the electronic/ionic flux and affect antioxidant enzyme capacity (Toduka et al., 2012; Sabella et al., 2014; Vinković Vrček et al., 2016; Milić et al. 2015). The *in vitro* toxic effects of AgNPs has been reported for a wide range of cell lines where increased oxidative stress, apoptosis and DNA damage have been found as the main cellular outcomes after treatment with AgNPs (Bondarenko et al., 2013; Gliga et al., 2014; Reidy et al., 2013). Biological consequences of interactions between living cells and NP strongly depend not only upon size, material, and surface characteristics, but also on the processes involved in cellular uptake of NP and their intracellular distribution (Liu et al., 2014; Toduka et al., 2012; Hsiao et al., 2014; Madani et al., 2011; Bannunah et al., 2014; Rothen-Rutishauser et al., 2014; Sabella et al., 2014; Vranic et al., 2013; Meindl et al., 2017; Verma and Stellacci, 2010). The internalization pathways of materials into cells are typically classified into clathrin- and caveolae-mediated endocytosis, phagocytosis, macropinocytosis, and pinocytosis (Liu et al., 2014; Toduka et al., 2012; Hsiao et al., 2014; Madani et al., 2011; Bannunah et al., 2014; Rothen-Rutishauser et al., 2014; Sabella et al., 2014; Vranic et al., 2013; Meindl et al., 2017; Iversen et al., 2011). Receptor-mediated endocytosis, including clathrin- and caveolae-mediated pathways, is the most important mechanism of internalization of nanoscale materials, including viruses and NP (Wang et al., 2012; Tomatis et al., 2010). Phagocytosis is an actin-dependent process by which specialized phagocytic cells internalize materials larger

than 0.5 μm (Aderem and Underhill, 1999). Pinocytosis is important cell pathway for translocation of fluids and small NP, while macropinocytosis is process by which cells internalize fluids and particles together forming large vesicles (0.2–5 μm) (Geiser, 2010; Oh and Park, 2014; Dutta and Donaldson, 2012).

Although numerous studies on cellular toxicity mediated by AgNP were conducted, there is still need to fill the knowledge gaps on mechanisms by which AgNP enter and affect cells (Verma and Stellacci, 2010; Landgraf et al., 2015; Geiser, 2010; Iversen et al., 2011; Sabella et al., 2014). At present, information regarding the role of surface-chemical properties on AgNP interactions with cells is still missing. Therefore, this study aimed (i) to investigate the impact of nanoparticle surface properties on cyto- and genotoxicity of AgNP in human hepatoma cells (HepG2) by assessing metabolic activity, cell viability and primary DNA damage, and (ii) to examine uptake mechanisms of AgNP by employing different inhibitors that block particular internalization routes. Differentially coated AgNP were prepared by surface functionalization using sodium bis(2-ethylhexyl)-sulfosuccinate (AOT), cetyltrimethylammonium bromide (CTAB), poly(vinylpyrrolidone) (PVP), poly-*L*-lysine (PLL), and bovine serum albumin (BSA). The HepG2 cell line was selected as it retains many of the genotypic and phenotypic features of normal liver parenchymal cells, including an intrinsic metabolism such as synthesis and secretion of plasma proteins (Knasmüller et al., 1998; Sussman et al., 2004). It has been already demonstrated that human hepatocellular cell lines may serve as good model for investigation of NP-induced responses in liver cells (Kermanizadeh et al., 2014; Kermanizadeh et al., 2016). Toxicity of different AgNP in HepG2 cells was determined by means of cell viability and DNA damage evaluation. Cellular uptake of different AgNP was quantified by flow cytometry. Uptake mechanism was evaluated in the presence of several pharmacologic inhibitors that disrupt specific uptake mechanism, *i.e.* phenylarsine oxide (PAO) as inhibitor of clathrin-mediated endocytosis,

cytochalasin D, nocodasole and amiloride as inhibitors of macropinocytosis, and filipin that inhibits caveolae-mediated endocytosis (Liu et al., 2014; Linares et al., 2014; Jiang et al., 2013; Toduka et al., 2012; Hsiao et al., 2014; Madani et al., 2011; Bannunah et al., 2014; Rothen-Rutishauser et al., 2014; Sabella et al., 2014; Vranic et al., 2013; Meindl et al., 2017; Oh and Park, 2014; Dutta and Donaldson, 2012).

2. Materials and methods

2.1.Chemicals and materials

Human Caucasian hepatocyte carcinoma (HepG2) cells from the European Collection of Cell Cultures (ECACC, Salisbury, UK) were used in this study. GIBCO® Minimum Essential Medium (MEM) was purchased from Thermo Fisher Scientific (Schwerte, Germany). Dulbecco's Phosphate Buffered Saline (PBS) medium, fetal bovine serum (FBS), bovine serum albumin (BSA) (product number A-7906), penicillin and streptomycin were purchased from Sigma–Aldrich Chemie GmbH (Steinheim, Germany). The plastic and glassware used for chemical analysis were from Sarstedt (Germany). The 3-(4,5-dimethylthiazol-2-yl)-2,5-diphenyltetrazolium bromide (MTT) assay kit was purchased from Roche Diagnostics GmbH (Germany). Osmium tetroxide was purchased from Agar Scientific (Stansted, UK) and TAAB epoxy resin (medium hard) from Aldermaston (Berkshire, UK). All other analytical grade chemicals were obtained from Sigma (Germany) and Merck (Germany). All dilutions were made with high purity deionized water (18.2 MΩcm), obtained from a Milli-Q® system (Merck Chemicals GmbH, Darmstadt, Germany).

2.2.Synthesis and characterization of AgNP

Differentially coated AgNP were prepared by surface functionalization using sodium bis(2-ethylhexyl)-sulfosuccinate (AOT), cetyltrimethylammonium bromide (CTAB), poly(vinylpyrrolidone) (PVP), poly-*L*-lysine (PLL), and bovine serum albumin (BSA) following established procedures described elsewhere (Vinković Vrček et al., 2015).

Characterization of AgNP was performed in both ultrapure water (UW) and cell culture medium (CCM), which was prepared as MEM supplemented with 10% (m/v) FBS. Total silver concentrations in AgNP were determined using an Agilent Technologies 7500cx inductively coupled plasma mass spectrometer (ICPMS) (Waldbronn, Germany) as described elsewhere (Vinković Vrček et al., 2015). The size and charge of AgNP were measured by dynamic (DLS) and electrophoretic light scattering (ELS), respectively, using Zetasizer Nano ZS (Malvern, UK). Visualization of AgNP and cells were conducted using a transmission electron microscope (TEM, Zeiss 902A, Oberkochen, Germany). TEM images were also used for confirmation of AgNP size obtained by DLS. Particles size was determined from the cross-sectional area of the particles which was converted to an equivalent spherical diameter by using Image J software. Primary particles were distinguished from AgNP aggregates by tracing it manually.

The possible AgNP dissolution in UW and CCM was determined by determining the dissolved silver ions using centrifugal ultrafiltration (Millipore Amicon Ultra-4 3K) through a membrane with a nominal molecular weight limit of 3 kDa. Suspensions were centrifuged for 30 min at 15000 × *g* (Eppendorf Microcentrifuge 5417R, Eppendorf AG, Hamburg, Germany). The Ag concentration in the filtrate as determined by ICPMS was related to the Ag concentration before ultrafiltration to calculate dissolved Ag fraction.

2.3.Cell culture

HepG2 cells were cultured in MEM medium, supplemented with 10% (m/v) FBS, 20 IU/ml penicillin and 20 μg/ml streptomycin. The cells were seeded in 6-, 24- or 96-well plates and maintained at 37 °C in a humidified atmosphere of 5% CO_2 in air. The medium was replaced every 2-3 days. Upon reaching 80% adherent confluence, cells were treated with a range of concentrations of AgNP suspended in the cell culture media (CCM). In each experiment, stock AgNP suspensions were freshly diluted to appropriate concentrations in CCM. Controls without treatment were performed for each analysis.

2.4.Cell viability assay

Metabolic activity in treated compared to control HepG2 cells was determined using the MTT assay based on reduction of the yellow tetrazolium salt MTT (3-(4,5-dimethylthiazol-2-yl)-2,5-diphenyltetrazoliumbromide) to a purple MTT-formazan crystal (Mosmann, 1983). Viable cells with active metabolism are able to reduce MTT into formazan, while dying cells lose this ability (Riss et al. 2006). Thus, MTT assay was used in this study to quantify the number of viable cells. Cells were seeded in 96-well tissue culture plates (5×10^4 cells/ml growth medium) followed by an overnight incubation. Different AgNP were added to quintuplicate wells to a final concentration range of 0 - 100 mg/L and incubated for another 24 hr. Doses of AgNPs were chosen based on previously published results (Vinković Vrček et al., 2016). Negative controls were untreated HepG2 cell, while positive controls were cells treated with 10% dimethyl sulfoxide (DMSO). At the end of treatment, the medium from each well was removed by aspiration; cells were washed 3 times with 200 μl PBS/well to remove all AgNP that may interfere with MTT assay (Vinković Vrček et al., 2015). Then, 50 μl of 1000 mg/L MTT solution was added to each well. After 4 hr incubation at 37 °C, the

MTT solution from each well was removed by aspiration. A volume of 50 µl DMSO was added and the plate was shaken to dissolve the MTT-formazan crystals. The optical density at 595 nm was then determined for each well using a Victor™ multilabel reader (Perkin Elmer, Massachusetts, USA). In addition, control plates with the same concentration range of AgNP were prepared, and the background absorbance of AgNP was subtracted on a plate reader to avoid false positive results that may lead to an underestimation of NP-induced toxicity (Vinković Vrček et al., 2015).

2.5.Flow cytometry experiments

Flow cytometry experiments were performed for determination of AgNP effects on the number of live and dead HepG2 cells, AgNP uptake efficiency and mechanisms of AgNP internalization, using Attune® acoustic focusing flow cytometer (Applied Biosystems, USA) with 488 nm laser. The cytometer was set up to measure FSC linearly and SSC logarithmically. The highest concentration of AgNP was run first to set the range for the maximum SSC signal. For the analysis on the flow cytometer, HepG2 cells were dissociated after each treatment using 0.05 % Gibco™ Trypsin-EDTA (Thermo Fisher Scientific) solution, washed with PBS, resuspended in PBS-based buffer containing 2% FBS and 2 mM EDTA (pH 7.4, filtered through 0,2 µM sterile filter) and passed through a 40 µm *Falcon*™ *cell strainer* (Thermo Fisher Scientific).

Cell viability was evaluated using Molecular Probes™ LIVE/DEAD™ Viability/Cytotoxicity kit (Invitrogen, Fisher Scientific). For the experiment, HepG2 cells were seeded in 6 well plates at a density 2.5×10^5 cells/well. Forty-eight hr after HepG2 plating, the culture medium was exchanged with a fresh one and increasing concentrations of AgNP added (1, 5 or 25 mg/L). Cells without AgNP treatment served as a negative control in

each experiment. Dissociated cells were incubated with 0.1 μM calcein acetoxymethyl ester (CAM) and 3 μM ethidium homodimer-1 (EthD), both supplied in the kit, for 15 min in the dark at the room temperature. Each experiment was repeated 3 times. CAM and EthD were measured using log amplifiers. The percentage of live HepG2 cells (CAM-positive and/or EthD-positive) was calculated using FCS Express 5 Flow Cytometry Software (De Novo Software, Glendale, USA).

To determine NP uptake efficiency, the % NP-labelled cells was determined using Attune acoustic focusing cytometer by measuring the increase of the side scattered light of the laser beam (SSC). The intensity of the SSC is proportional to the intracellular density and granularity (Zucker and Daniel 2012). Uptake of NP into cells increases the SSC intensity by enhancing the intracellular density. The % of positive cells (compared to the control) was determined with FCS Express 5 Flow Cytometry Software using Overton cumulative histogram subtraction method (Overton 1988).

Mechanism of AgNP internalization in HepG2 cell was investigated using inhibitors that block specific cell uptake route. Before starting the investigation of uptake mechanism, the effect of inhibitors on HepG2 cell viability was tested in order to find a proper inhibitor dose. The dose of each inhibitor was chosen according to the previously published literature (Jiang et al., 2013; Gliga et al. 2014; Hsiao et al. 2014). All inhibitors exhibited negligible cytotoxicity at the dose 5 times higher than the dose selected for the study of uptake mechanism. Following inhibitors were applied: cytochalasin D at the dose of 0.3 μM as inhibitor for actin-dependent pathways, phenylarsine oxide (PAO) at the dose of 30 nM as inhibitor of clathrin-mediated endocytosis, nocodazole at the dose of 20 nM as inductor of microtubule disruption, filipin at the dose of 1.5 mg/L as inhibitor of caveolin-mediated endocytosis, and amiloride hydrochloride hydrate at the dose of 0.15 mM as inhibitor of macropinocytosis. All inhibitors were purchased from Sigma. HepG2 cells were pre-treated

with the above inhibitors for 30 min and then incubated with 5 mg/L AgNP for additional 4 hr in the presence of the inhibitor. Two control cells were used for final evaluation: (i) cells without inhibitors and without AgNP, and (ii) cells treated only with 5 mg/L AgNP but without pretreatment with inhibitors. The effect of inhibitors on cellular AgNP uptake was examined using Attune acoustic focusing cytometer.

2.6.DNA damage evaluation

DNA damage in HepG2 cells treated with different AgNP was assessed by alkaline comet assay (Singh et al., 1988; Tice et al., 2000). HepG2 cells were seeded in 24-well plates at a density 10^3 cells/ml, and maintained in the CCM at 37°C in a humidified atmosphere of 5% CO_2 in the air. The medium was replaced every 2-3 days. Upon reaching 70% confluence, the CCM was changed to MEM without FBS supplementation to gain cells synchronisation. After 12 hr, cells were treated for 24 hr with different concentrations of AgNP suspended in the CCM. Cells treated with the CCM were used as negative control, while cells treated with DMSO were used as positive control. All experiments have been performed in replicates. For each experiment, 2 slides per concentration were prepared. At the end of exposure period, the genotoxicity end points in the control and exposed single cells were evaluated using alkaline comet assay technique (Singh et al. 1988; Tice et al. 2000). The parameters selected for quantification of DNA damage were: a comet tail length (TL, in µm, calculated from the centre of the head of the comet) and tail intensity (TI, % DNA in comet tail). The extent of DNA damage, as recorded by the alkaline comet assay, was analysed considering the mean, standard deviation of the mean, median and range of the comet parameters measured. Experiments were done in duplicate and analysed for statistical differences compared to negative control. In total 220 comets were measured for each particle type and concentration.

2.7.Visualisation of HepG2 cells treated with AgNP

After 24 hr treatment of HepG2 cells with 5 mg/L AgNP, cells were detached from the wells using trypsin for 7 min, washed once with CCM, separated by centrifugation and fixed overnight with 2% glutaraldehyde in 0.1 M phosphate buffer, post-fixed in 1% osmium tetroxide, and contrasted in 2% uranyl acetate in water. Samples were dehydrated in acetone and embedded in Durcupan (Sigma-Aldrich, Germany). The ultrathin sections were cut on RMC Power Tome XL (Boeckeler Instruments, USA) ultramicrotome. TEM samples were prepared by depositing ultrathin sections on a Formvar® coated copper grid, contrasted with uranyl acetate and lead citrate and examined on transmission electron microscope Zeiss 902A (Oberkochen, Germany) operated in the bright field mode at an acceleration voltage of 80 kV. Images were recorded with Canon PowerShot S50 digital camera attached to the microscope.

2.8.Statistical analysis

Differences between measured variables were tested using simple and repeated measures ANOVA, followed by Fisher LSD *post hoc* test and level of significance set at $P < 0.05$. Data were log transformed if required to meet assumptions of ANOVA, and homogeneity of variances was tested using the Levene's test. In other cases, differences were tested using the Dunnett test (to assess differences versus a control), or Kruskal-Wallis ANOVA of ranks (non-parametric test used when assumptions of homogeneity of variances were not feasible). All statistical analyses were carried out using STATISTICA v9.0 (StatSoft, Inc., Tulsa, USA).

3. Results

3.1.Characterization and stability evaluation of AgNP

Evaluation of characteristics and dispersion behaviour of differently coated AgNP in both UW and CCM was performed using DLS, ELS, TEM and ICPMS techniques (Table 1 and Figs. 1-2). DLS measurements and TEM evaluation in UW showed that size distributions were monomodal only for AOTAgNP, while other AgNP were characterized by bimodal volume-weighted size distributions (Table 1). Furthermore, CTABAgNP showed three size populations. In relation to size, most AgNP had hydrodynamic diameters (d_H) in range 5 - 20 nm. Visualization of the AgNP by TEM evidenced spherically shaped NPs (Fig. 1). The ELS data confirmed assumption that charge of coating agent determines also ζ potential values of AgNP in UW (Fig. 2). Thus, functionalization with PLL and CTAB led to positively charged AgNP characterized by a ζ potential of 24.2 ± 3.7 and 38.7 ± 4.2 mV, respectively. The use of negatively charged AOT resulted in ζ potential of -28.1 ± 1.9 mV, while PVPAgNP and BSAAgNP were characterized by -18.9 ± 1.7 and -6.1 ± 0.7 mV, respectively. Negative ζ potential of former can be explained by the use of borohydride during synthesis of PVPAgNP leading to adherence of the BH_4^- anions to the NP surface.

In the CCM, the presence of FBS stabilized AgNP as can be seen in Table 1. Although all AgNP types aggregated slightly upon immersion in CCM, observed size distribution diagrams did not show aggregates larger than 200 nm as reported for the cell-culture medium without proteins (Domazet Jurašin et al., 2016). Obtained DLS data were confirmed by TEM evaluation (Table 2). Measured ζ potentials in the CCM ranged from -10.2 to -14.3 mV, close to the ζ potential of serum albumin (~ -7 mV), one of the main component of FBS supplement, which indicated that protein coating provided stability to all AgNP types in the CCM.

Results on dissolution of AgNP in the UW and CCM, as evaluated by measuring total Ag content after filtration of AgNP through membranes of 3 kDa pore size, clearly show that Ag^+ content was lower than 5% in all AgNP types (Table 1). The lowest dissolution was observed for PLLAgNP, i.e. ~ 1% in the UW and 0.7% in the CCM. The highest Ag^+ content was observed for the BSAAgNP, i.e. 3.3 and 4.2% in the UW and CCM, respectively. AgNP coated with AOT, BSA, and CTAB had higher Ag^+ level in the CCM compared to the UW, i.e. 0.2, 3.3 and 0.4% vs. 1.2, 4.2 and 1.1%, respectively. Only PVPAgNP showed lower Ag^+ fraction in the CCM compared to the UW.

3.2.Toxicity effects of different AgNP types

Cytotoxicity of different AgNP types in HepG2 cells was assessed by means of cell metabolic activity corresponding to the cell viability (MTT assay), by evaluating the number of live and dead cells (LIVE/DEAD^{TM} Viability/Cytotoxicity) and by the extent of primary DNA damage (alkaline comet assay).

The MTT assay was applied to demonstrate HepG2 viability. The non-treated cells were considered as negative control showing viable cells (Fig. 3). Dose-response decrease in metabolic activity was observed for all AgNP types. BSAAgNP showed the highest toxic effect and decreased cell viability by 50% already at the dose of 5 mg Ag/L. The effective concentrations for 50% of cell loose at 24 hr were calculated to be 25 mg Ag/L for both PLLAgNP and CTABAgNP (Fig. 3). Same concentrations of PVPAgNP and AOTAgNP decreased cell viability by 75 and 58%, respectively.

The results obtained using LIVE/DEAD^{TM} Viability/Cytotoxicity assay was standardized on the number of stained cells showing consistently dose-response effects of AgNP (Fig. 4). Again, BSAAgNP induced highest cell mortality at the applied doses of 5 and

25 mg Ag/L compared to other types of AgNP, whereas percentages of live and dead cells were comparable for all others AgNP.

The alkaline comet assay was used to determine the DNA damage due to the AgNP treatment. The exposure to up to 10 mg Ag/L of AgNP for 24 hr led to the primary DNA damage in HepG2 cells (Table 2). No significant increase in the percentage of DNA in the comet TL was observed after exposure to the lowest dose of AgNP (Table 2). However, significant increase in comet TI was measured at the lowest dose of PVPAgNP. At the highest applied dose (10 mg/L), the highest increase in both comet TL and TI was induced by PLLAgNP followed by AOTAgNP, while CTABAgNP appeared to induce the lowest extent in DNA damage in HepG2 cells.

3.3.Visualisation of AgNP uptake by TEM

TEM visualisation of treated HepG2 cells clearly indicated cellular uptake of AgNP. Fig. 5 showed that all AgNP types were found mainly within membrane-bound structure. The other cellular compartments such as nucleus, endoplasmatic reticulum or Golgi apparatus did not contain any of AgNP. PVP-, BSA- and CTABAgNP were observed as condense clusters inside membrane limited vesicles inside the cells (Fig. 5). It appears that BSAAgNP were capable of escaping from membrane-limited vesicles and reach mitochondria (Fig. 8f). In the case of PLL- and AOTAgNP, they were taken up by HepG2 cells not only as clusters, but also as individual particles.

3.4.Cellular uptake of different AgNP types

The quantification of the uptake of different AgNP by HepG2 cells was analyzed by flow cytometry measuring the increase of the side scattered light (SSC) of the laser beam. The

SSC intensity is proportional to the intracellular density, and therefore correlates with the AgNP uptake (Liu et al., 2014; Toduka et al., 2012). Currently, there are no standardized and validated methods for the undoubtful quantification of NP uptake into cells (Drasler et al., 2017). Flow cytometry cannot distinguish AgNP internalized into the cell from those just attached to the cell surface, but this limitation may be compensated when flow cytometry is combined with microscopic techniques (Drasler et al., 2017). Indeed, TEM images demonstrated uptake of all AgNP by HepG2 cells (Fig. 5). Thus, flow cytometry data were discussed within this study in the context of semiquantitative analysis of AgNP cellular uptake.

Internalization of all AgNP types in HepG2 cells followed dose-response curve (Fig. 6). Obtained results showed different cellular uptake for differently coated AgNP (Fig. 6). The most pronounced uptake was observed for PLLAgNP. At the highest applied dose of 25 mg Ag/L, more than 80% of . Thus cells internalized PLLAgNP. Uptake of CTAB-, PVP- and AOTAgNP was similar and somewhat weaker compared to the PLLAgNP, leading to the AgNP internalisation in ~ 50% HepG2 cells at the highest applied dose (Fig. 6). Only BSAAgNP showed the internalization lower than 30% (Fig. 6). Uptake of PLLAgNP was obviously promoted by interaction of positively charged PLL on the NP surface with negatively charged cell surface.

The uptake mechanisms were analyzed by different inhibitors that block particular internalization route as previously described (Liu et al., 2014; Toduka et al., 2012; Hsiao et al., 2014; Madani et al., 2011; Bannunah et al., 2014; Rothen-Rutishauser et al., 2014; Sabella et al., 2014; Vranic et al., 2013; Meindl et al., 2017; Oh and Park, 2014; Dutta and Donaldson, 2012). Nocodazole and filipine did not exhibit a significant change in the uptake of any AgNP type compared to the control cells. Next, pretreatment of HepG2 cells with the amiloride resulted in > 30% inhibition rate for PVP-, BSA- and CTABAgNP, while uptake of AOT- and

PLLAgNP was inhibited by < 30% by this inhibitor (Fig. 7). Cytochalasin D, inhibitor of actin dependent pathways, reduced the uptake rate by more than 50% for all AgNP types, while this inhibition rate was more than 75% for the AOT- and PVPAgNP (Fig. 7). Similar inhibition results were obtained when using PAO as inhibitor of clathrin-mediated endocytosis. Uptake of AOT-, PVP- and CTABAgNP were reduced by > 80%, while internalisation of BSA- and PLLAgNP were decreased by > 50% after pretreatment with PAO. According to these results, macropinocytosis and clathrin-mediated endocytosis are primary uptake pathways for all tested AgNP.

4. Discussion

4.1. Stability of AgNP in cell culture media

Data presented in Table 1 and Fig. 1 indicate that coating agent determine the nature of AgNP colloidal system. Not all coating agent are capable to stabilize AgNP accurately enough for the preparation of monodisperse NP system. In this study, we applied the classical bottom-up synthetic approach using sodium borohydride to reduce $AgNO_3$ that was described in numerous publications as simple preparatory procedure for monodisperse AgNP system (Evanoff and George, 2005; Tejamaya et al., 2012; Solomon et al., 2007; Lee and Meisel, 1982; Nallathamby et al., 2008; Nallathamby and Xu, 2010). However, our results clearly show that the selection of coating agent is critical step during AgNP synthesis. Different coating agent may affect size and shape of NP either by changing the relative growth rates of NP seeds to nanocrystals or by performing different coverage density on the AgNP surface.

Prior to any investigation of biological effects induced by NP, careful characterization and stability evaluation of nanomaterials should be performed under relevant experimental condition (Domazet Jurašin et al., 2016; Kerminazideh et al., 2016). Forces between NP and

components in biological media strongly influence aggregation behaviour of nanomaterial leading to completely different behaviour of aggregated or agglomerated NPs within biological systems compared to single NP (Domazet Jurašin et al., 2016). In addition, NP surface chemistry is in dynamic interaction with various biomolecules present in biological solutions, such as blood, saliva, and cell culture media (Sharma et al., 2014; Zook et al. 2011). The proteins covering the nanoparticle surface further prevent the individual NP from aggregation or agglomeration (Treuel et al., 2014).

As we already reported for behaviour of the same types of AgNP in the cell culture media supplemented with 0.1% (m/v) bovine serum albumin (Domazet Jurašin et al., 2016), the presence of proteins in the CCM prevented massive agglomeration of AgNP. Although all AgNP types aggregated slightly upon immersion in the CCM (Table 1), observed size distribution diagrams did not show aggregates larger than 200 nm as reported for the cell-culture medium without proteins (Domazet Jurašin et al., 2016). All AgNP showed similar hydrodynamic radii upon suspension in the CCM, ranging from 47 to 87 nm (Table 1). This is clear indication of protein corona formation on the surface of AgNP which leaded to the increased d_H compared to the UW. Only PLLAgNP showed the significant amount of 200 nm-sized clusters in the CCM. However, TEM values for PLLAgNP clearly demonstrated that these are not real NP aggregates, rather assembles of protein covered AgNP and free PLL in the CCM. As evidenced by the TEM values for the AgNP diameter (Table 1), all AgNP showed decreased size of the metal core in the CCM compared to the UW. Thus, protein corona obviously prevented aggregation of all AgNP types in the CCM.

Surface functionalisation significantly influenced dissolution behaviour of all AgNP types except for PLLAgNP (Table 1). Increased level of Ag^+ in the CCM compared to the UW was found for AOT-, BSA-, and CTABAgNP, whereas suspension of PVPAgNP in the

CCM inhibited dissolution compared to the UW. The highest Ag^+ content was observed for the BSAAgNP.

4.2.Cyto- and genotoxicity of different AgNP

Obtained results clearly showed different toxic potential of AgNP having different surface functionalization. This corresponded well with recent observation in animal models where citrate-coated AgNP induced significantly higher histopathological alterations in fish gill compared to PVP-coated AgNP (Hawkins et al., 2015). All AgNP types showed dose dependent effects on HepG2 cells. As measured by LIVE/DEAD™ and MTT assays, toxic potential of differently coated AgNP followed the order of BSAAgNP > PLLAgNP > CTABAgNP > AOTAgNP > PVPAgNP. However, flow cytometry experiments using LIVE/DEAD™ assay indicated lower survival rate than what could be assumed from the results obtained by MTT. The reason for these differences could be residual interference which may be induced by the presence of not removed NP during MTT assay. Thus, lower cell survival measured by flow cytometry can indicate that MTT assay could be biased toward more positive results than the real viability (Vinković Vrček et al., 2015). The interference issues and the proper combinations of *in vitro* assessment techniques were already proven as extremely important for cytotoxicity evaluations of NPs (Vinković Vrček et al., 2015).

Positively charged compared to negatively charged AgNP showed significantly higher toxicity as measured by LIVE/DEAD™ and MTT assays. The reason may be the differences in more efficient electrostatic interaction between the positively charged NP and negatively charged cell membranes (Bannunah et al., 2014). Interestingly, the most "to-be-biocompatibile" NP – BSAAgNP – were shown as the most "aggressive" for survival rate and cellular viability of HepG2 cells. This may be explained by the highest rate of dissolution behaviour found for BSAAgNP. The obtained results are consistent with previously reported

observation in mammalian liver cells (Vinković Vrček et al., 2016; de Lima et al. 2012; Arora et al., 2009; Avalos et al., 2014).

Genotoxicity evaluation of different AgNP types using the alkaline comet assay showed primary DNA damage in HepG2 cells due to the exposure to non-cytotoxic concentrations of AgNP. In all treated cells, the amount of DNA damage followed dose-response pattern. Highest extent in the primary DNA damage was found in HepG2 cells treated with PLLAgNP, while CTABAgNP showed the lowest genotoxic potential. It is important to stress that TL and TI parameters showed similar dynamics of DNA damage as induced by AgNP.

In spite of numerous studies on AgNP effects on mammalian cells and tissues, there is still debate about "Trojan horse" effect as the main reason of AgNP biological effects (Gliga et al., 2014). Thus, it is still not clearly established whether nanoparticles per se induced toxicity or Ag^+ ions that could be released from the AgNP surface in certain biological media. In previous study, we showed that the effective concentrations of ionic Ag for 50% HepG2 cell loss at 24 hr (EC50 values), as measured by the MTT assay, were calculated as 0.5 mg/L, while 1 mg/L of Ag^+ decreased cell viability by 62% (Vinković Vrček et al., 2016). As ionic Ag exhibited such strong cytotoxicity in HepG2 cells, dissolution behaviour of each AgNP used in this study was evaluated (Table 1). If we assume that AgNP dissolve the same amount of Ag^+ inside the cells and in the CCM above the cells, as it was observed in the CCM supplemented with 10% (m/v) FBS, then cytotoxicity effects observed for AOT-, PVP- and BSAAgNP may be partially explained by release of ionic Ag from their surface (Table 1 and Figure 3). However, for the CTAB- and PLLAgNP, magnitude of cytotoxic effects was significantly higher than what can be expected from released Ag^+. Thus, nanoparticulate form should account for observed toxicity, particularly in the case of positively charged AgNP.

4.3.Uptake mechanism of differentially coated AgNP

In order to determine if different cytotoxic response of HepG2 cells could be due to the differences in cellular uptake of AgNP, flow cytometry and TEM imaging techniques were applied. This combination may provide better analysis for determination of uptake mechanism and localisation of NP inside the cells (Drasler et al., 2017). All techniques that can be used to evaluate NP cellular uptake have inherent limitation that it is not possible to differentiate between NP that are inside cells or on the cell surface (Drasler et al., 2017). Compared to image analysis, flow cytometry has advantage due to a rapid, easy and high-volume analysis of cells, while transmission electron microscopy may be used to approve NP in endosomes. Thus, inherent limitation of flow cytometry may be counterbalanced when it is combined with the TEM analysis (Drasler et al., 2017).

As for cytotoxicity effects, dose response was also observed for cellular uptake of different AgNP (Fig. 6). The uptake was more promoted for positively charged AgNP due to electrostatic interaction with negatively charged cell surface. Although the neutral and negative functional groups may prevent NP–biological interactions (Verma and Stellacci, 2010), uptake of PVP- and AOTAgNP were similar. The reason may arise from nonspecific binding of proteins from the CCM to surfaces of both AgNP types leading to favourable interaction with cell membrane and their active transport inside the cells. It has been already shown that uptake of negatively charged NPs is successful despite the unfavourable electrostatic interaction with negatively charged cell membrane (Verma and Stellacci, 2010; Bannunah et al., 2014). The lowest internalization observed for BSAAgNP could be explained by weak ability of HepG2 cells for receptor-mediated endocytosis (Christensen and Birn, 2002).

Uptake of AgNP may be also discussed in terms of their aggregation behaviour. However, all AgNP had similar d_H in the CCM (Table 1) caused by the protein corona

formation, which finally governed their interaction with cells. Only PLLAgNP showed in the CCM significant amount of NP population bigger than 100 nm. Indeed, the highest uptake rate of PLLAgNP may be explained be the observed aggregation behaviour. The rapid settling of aggregated PLLAgNP may increase their local concentration close to the cell surface enhancing their uptake into the HepG2 cells. Thus, aggregation behaviour of NP should be always taken into account during investigation of their uptake or interaction with cells.

The uptake mechanism of different AgNP types was investigated by using pharmacologic inhibitors. Use of inhibitors that suppress specific endocytic pathway is well described approach to elucidate the endocytic mechanisms; amiloride inhibits the Na^+/H^+ exchange required for macropinocytosis, cytochalasin D inhibits macropinocytosis by blocking actin polymerization avoiding microfilaments action, PAO affects clathrin-mediated endocytosis by decreasing membrane fluidity, filipine blocks caveolin-mediated endocytosis by binding on cholesterol in the membrane and inhibiting the formation of caveolae rafts in cholesterol-rich regions, nocodazole disrupts microtubule participation in the uptake (Liu et al., 2014; Toduka et al., 2012; Hsiao et al., 2014; Madani et al., 2011; Bannunah et al., 2014; Rothen-Rutishauser et al., 2014; Sabella et al., 2014; Vranic et al., 2013; Meindl et al., 2017). To determine mechanism of AgNP uptake using different inhibitors, the uptake was measured only after short exposure time (4 hr), since blocking of one uptake pathway can result in activation of other mechanisms, which may confound the overall result (Verma and Stellacci, 2010; Liu et al., 2014; Rothen-Rutishauser et al., 2014; Sabella et al., 2014; Vranic et al., 2013). Thus, it was critical to find the sufficient time for both, the detectible NP amount inside the cells and blocking of endocytosis by inhibitors applied. Another important factor was concentration of inhibitor which should be adequate for blocking action, but not enough to induce cell toxicity.

Results obtained using different inhibitors clearly showed that all AgNP types were taken by HepG2 cells by a combination of different active mechanisms (Fig. 8) including clathrin-mediated, actin-dependent endocytosis, macropinocytosis (Koivusalo et al., 2010; Nam et al., 2009; Oh and Park, 2014; Dutta and Donaldson, 2012; Liu et al., 2014; Gliga et al. 2014). Neither nocodazole, which disrupts microtubule participation, nor filipine, which binds on cholesterol in the membrane and inhibits the formation of caveolae rafts in cholesterol-rich regions, exhibited any significant change in the uptake of any of the AgNP type studied here compared to the control cells. Thus, caveolae-associated endocytosis and microtubule participation were not involved in the uptake of studied AgNP by HepG2 cells. However, the absence of caveosomes are already reported in the literature for the HepG2 cells (Jiang et al. 2013), which could be the main reason why we could not observe any caveolae-mediated pathway. Interestingly, microfilaments action through actin polymerisation and clathrin-coated vesicles obviously have important role in internalisation of all studied AgNP as demonstrated by inhibitory effects of cytochalasin D and PAO, respectively. Inhibition of Na^+/H^+ exchange required for macropinocytosis was observed for the PVP-, BSA and CTABAgNP treated cells after pretreatment with amiloride. Interestingely, the incubation of cells with negatively charged AOT- and positively charged PLLAgNP showed similar uptake behaviour (Fig. 7). The uptake of these two AgNP were inhibited only by pretreatment of HepG2 cells with cytochalasin D and PAO, which suggested a clathrin- and macropinocytosis-dependent mechanisms (Fig. 7). Internalization of BSAAgNP was decreased by amiloride to a much lesser extent compared to pretreatment with cytochalasin D and PAO, implying more pronounced macropinocytosis compared to endocytosis. Macropinocytosis was the most important pathway for PVPAgNP, where amiloride, an inhibitor of macropinocytosis, and cytochalasin D, inhibitor of actin polymerisation, decreased their uptake much more than in the case of other AgNP. For AOTAgNP,

pretreatment with PAO induced almost complete inhibition of this clathrin-mediated uptake, indicating that specific NP-cell interactions played pronounced role for the negatively charged AgNP. As surface charge showed no clear trend, polydispersity and agglomeration state together with the protein corona formation on the AgNP surface affected the internalization pattern of AgNP by HepG2 cells. Indeed, relative cellular uptake was similar for negatively and positively charged AgNP, while pronounced aggregation behaviour of PLLAgNP in the CCM might affect their transfer into the cells. Highest % of relative uptake of PLLAgNP as measured by flow cytometry may be artefact, as the increase in the SSC intensity may be also induced by the NP attached to the cell surface.

TEM visualization evidenced that all AgNP types were taken up and contained mainly within endosomes and lysosomes (Fig. 5). TEM images also demonstrated that all AgNP types may interact with the cell membrane in the form of clusters which were endocytosed by the cells. Surface functionalization was again found as important factor which defines intracellular localization and trafficking of AgNP. Although all techniques that can be used to study uptake mechanism of NP are limited by the fact that it is not possible to undoubtly distinct between taken and plasma membrane attached NP, images presented in Fig. 5 clearly show that all AgNP types were found within membrane-bound cellular structures. Thus, we may discuss only about the right quantity of AgNP taken up in HepG2 cells as measured by flow cytometry. Our results are well in agreement with recent studies showing that all NP use multiple pathways to enter into mammalian cells (Bannunah et al., 2014).

5. Conclusion

As demonstrated in this study, AgNP had the capacity to interact with the mammalian cells and enter them easily by different energy driven internalisation pathways (Fig. 8). The

main uptake mechanisms of AgNP coated with PVP, AOT, PLL, CTAB and BSA were macropinocytosis and clathrin-mediated endocytosis. None of the pharmacological treatments could fully inhibit NP uptake indicating that AgNP entered into mammalian cells by multiple pathways. Surface functionalization was demonstrated to be the important factor determining the toxicity and mechanism of AgNP uptake. However, the agglomeration state, the presence of specific receptors on cell surface, the composition of protein corona on NP surface, should be also taken into account when elucidating the mechanism of NP internalisation. The results clearly indicated the importance of careful analysis and individual interpretation for each cell-NP system in further development of nanotechnological applications.

Notes: The authors declare no competing financial interest.

References

Aderem, A., Underhill, D. M. 1999. Mechanisms of phagocytosis in macrophages. *Annu. Rev. Immunol.* 17, 593–623.

Arora, S., Jain, J., Rajwade, J. M., and Paknikar, K. M. 2009. Interactions of silver nanoparticles with primary mouse fibroblasts and liver cells. *Toxicol. Appl. Pharmacol.* 236, 310–318.

Avalos, A., Haza, A. I., Mateo, D., and Morales, P. 2014. Cytotoxicity and ROS production of manufactured silver nanoparticles of different sizes in hepatoma and leukemia cells. *J. Appl. Toxicol.* 34, 413–423.

Bannunah, A. M., Vllasaliu, D., Lord, J., and Stolnik, S. 2014. Mechanisms of nanoparticle internalization and transport across an intestinal epithelial cell model: effect of size and surface charge. *Mol Pharm.* 11(12), 4363-4373.

Bondarenko, O., Juganson, K., Ivask, A., Kasemets, K., Mortimer, M., and Kahru, A. 2013. Toxicity of Ag, CuO and ZnO nanoparticles to selected environmentally relevant test organisms and mammalian cells *in vitro*: A critical review. *Arch. Toxicol*. 87, 1181–1200.

Christensen, E. I., and Birn, H. 2002. Megalin and cubilin: Multifunctional endocytic receptors. *Nature* 3, 258–268.

de Lima, R., Seabra, A. B., and Durán, N. 2012. Silver nanoparticles: A brief review of cytotoxicity and genotoxicity of chemically and biogenically synthesized nanoparticles. *J. Appl. Toxicol.* 32, 867–879.

Domazet Jurašin, D., Ćurlin, M., Capjak, I., Crnković, T., Lovrić, M., Babič, M., et al. 2016. Surface coating affects behavior of metallic nanoparticles in a biological environment. *Beilstein J. Nanotechnol.* 7, 246–262.

Drasler, B., Vanhecke, D., Rodriguez-Lorenzo, L., Petri-Fink, A., and Rothen-Rutishauser, B. 2017. Quantifying nanoparticle cellular uptake: which method is best? *Nanomedicine (Lond)*. 12(10), 1095-1099

Dutta, D., and Donaldson, J. G. 2012. Search for inhibitors of endocytosis. Intended specificity and unintended consequences. *Cell. Logistics* 2, 203–208.

Evanoff Jr., D. D., and Chumanov, G. 2005. Synthesis and Optical Properties of Silver Nanoparticles and Arrays. *ChemPhysChem* 6, 1221-1231.

Geiser, M. 2010. Update on macrophage clearance of inhaled micro- and nanoparticles. *J. Aerosol. Med. Pulm. Drug Deliv*. 23, 207–217.

Gliga A. R., Skoglund S., Wallinder I. O., Fadeel B. and Karlsson H. L. 2014. Size-dependent cytotoxicity of silver nanoparticles in human lung cells: the role of cellular uptake, agglomeration and Ag release. *Part. Fibre Toxicol.* 11:11.

Hawkins, A. D., Thornton, C., Kennedy, A. J., Bu, K., Cizdziel, J., Jones, B. W., et al. 2015. Gill histopathologies following exposure to nanosilver or silver nitrate. *J. Toxicol. Environ. Health A.* 78, 301–315.

Hsiao, I., Mareike Gramatke, A., Joksimovic, R., Sokolowski, M., Gradzielski, M., and Haase, A. 2014. Size and Cell Type Dependent Uptake of Silica Nanoparticles. *J. Nanomed. Nanotechnol.* 5, 248. doi: 10.4172/2157-7439.1000248.

Iversen, T. G., Skotland, T., and Sandvig, K. 2011. Endocytosis and intracellular transport of nanoparticles: Present knowledge and need for future studies. *Nano Today*. 6, 176–185.

Jiang L., Li X., Liu L. and Zhang Q. 2013. Cellular uptake mechanism and intracellular fate of hydrophobically modified pullulan nanoparticles. *Int. J. Nanomed*. 8, 1825-1834.

Kermanizadeh, A., Gaiser, B. K., Johnston, H., Brown, D. M., and Stone, V. 2014. Toxicological effect of engineered nanomaterials on the liver. *British J. Pharmacol.* 171, 3980–3987.

Kermanizadeh, A., Gosens, I., MacCalman, L., Johnston, H., Danielsen, P. H., Jacobsen, N. R., et al. 2016. A multilaboratory toxicological assessment of a panel of 10 engineered nanomaterials to human health—ENPRA Project—the highlights, limitations, and current and future challenges. *J. Toxicol. Environ. Health B.* 19, 1–28.

Knasmüller, S., Parzefall, W., Sanyal, R., Ecker, S., Schwab, C., Uhl, M., et al. 1998. Use of metabolically competent human hepatoma cells for the detection of mutagens and antimutagens. *Mutat. Res*. 402, 185–202.

Koivusalo, M., Welch, C., Hayashi, H., Scott, C. C., Kim, M., Alexander, T., et al. 2010. Amiloride inhibits macropinocytosis by lowering submembranous pH and preventing Rac1 and Cdc42 signaling. *J. Cell Biol*. 188, 547–563.

Landgraf, L., Müller, I., Ernst, P., Schäfer, M., Rosman, C., Schick, I., et al. 2015. Comparative evaluation of the impact on endothelial cells induced by different nanoparticle structures and functionalization. *Beilstein J. Nanotechnol*. 6, 300–312.

Lee, P. C., and Meisel, D. 1982. Adsorption and Surface-Enhanced Raman of Dyes on Silver and Gold Sols. *J. Phys. Chem*. 86, 3391-3395.

Linares J., Matesanz M. C., Vila M., Feito M. J., Gonçalves G., Vallet-Regĭ M., Marques P. A. A. P. and Portolés M. T. 2014. Endocytic mechanism of graphene oxide nanosheets in osteoblast, hepatocytes and macrophages. *ACS Appl. Mater. Interfaces* 6, 13697-13706.

Liu, P., Sun, Y., Wang, Q., Sun, Y., Li, H., and Duan, Y. 2014. Intracellular trafficking and cellular uptake mechanism of mPEG-PLGA-PLL and mPEG-PLGA-PLL-Gal nanoparticles for targeted delivery to hepatomas. *Biomaterials* 35, 760-770.

Madani, F., Lindberg, S., Langel, Ü., Futaki, S., and Gräslund, A. 2011. Mechanisms of Cellular Uptake of Cell-Penetrating Peptides. *J Biophys.* 2011, 414729. doi: 10.1155/2011/414729.

Meindl, C., Öhlinger, K., Ober, J., Roblegg, E., and Fröhlich, E.2017. Comparison of fluorescence-based methods to determine nanoparticle uptake by phagocytes and non-phagocytic cells in vitro. *Toxicology* 378, 25-36.

Milić, M., Leitinger, G., Pavičić, I., Zebić Avdičević, M., Dobrović, S., Goessler, W. Et al. 2015. Cellular uptake and toxicity effects of silver nanoparticles in mammalian kidney cells. *J. Appl. Toxicol. 35,* 581−592.

Mosmann, T. 1983. Rapid colorimetric assay for cellular growth and survival: application to proliferation and cytotoxicity assays. *J. Immunol. Methods*. 65, 55−63.

Mulfinger, L., Solomon, S. D., Bahadory, M., Jeyarajasingam, A. V., Rutkowsky, S. A., and Boritz, C., 2007. Synthesis and Study of Silver Nanoparticles. *J. Chem. Educ.* 84(2), 322.

Nam, H. Y., Kwon, S. M., Chung, H., Lee, S. Y., Kwon, S. H., Jeon, H., et al. 2009. Cellular uptake mechanism and intracellular fate of hydrophobically modified glycol chitosan nanoparticles. *J. Control Rel*. 135, 259–267.

Nallathamby, P. D., Lee, K. J., and Xu, X.-H. N. 2008. Design of Stable and Uniform Single Nanoparticle Photonics for In Vivo Dynamics Imaging of Nanoenvironments of Zebrafish Embryonic Fluids. *ACS Nano*, 2, 1371-1380.

Nallathamby, P. D., and Xu, X.-H. N. 2010. Study of cytotoxic and therapeutic effects of stable and purified silver nanoparticles on tumor cells. *Nanoscale*. 2(6), 942-952

Oh, N., and Park, J. H. 2014. Endocytosis and exocytosis of nanoparticles in mammalian cells. *Int. J. Nanomed.* 9 (Suppl 1), 51–63.

Overton, W. 1988. Modified histogram subtraction technique for analysis of flow cytometry data. *Cytometry* 9, 619–626.

Paul, D., Achouri, S., Yoon, Y.-Z., Herre, J., Bryant, C. E., and Cicuta, P. 2013. Phagocytosis Dynamics Depends on Target Shape. *Biophys. J.* 105, 1143-1150.

Reidy B., Haase A., Luch A., Dawson K. A. and Lynch I. 2013. Mechanisms of Silver Nanoparticle Release, Transformation and Toxicity: A Critical Review of Current Knowledge and Recommendations for Future Studies and Applications. *Materials* 6, 2295-2350.

Riss T. L, Moravec R. A., O'Brien, M. A., Hawkins, E. M. and Niles, A. 2006. Homogeneous Multiwell Assays for Measuring Cell Viability, Cytotoxicity and Apoptosis. In: *Handbook of Assay Development in Drug Discovery*, ed. L. K. Minor. CRC Press, pp 385–406.

Rothen-Rutishauser, B., Kuhn, D.A., Ali, Z., Gasser, M., Amin, F., Parak, W.J., Vanhecke, D., Fink, A., Gehr, P., and Brandenberger, C. 2014. Quantification of gold nanoparticle cell uptake under controlled biological conditions and adequate resolution. Nanomedicine (Lond). 9(5), 607-621.

Sabella, S., Carney, R. P., Brunetti, V., Malvindi, M. A., Al-Juffali, N., Vecchio, G., Janes, S. M., Bakr, O. M., Cingolani, R., Stellacci, F., and Pompa, P. P. 2014. A general mechanism for intracellular toxicity of metal-containing nanoparticles. *Nanoscale* 6, 7052-7061.

Sharma, V. K., Siskova, K. M., Zboril, R., and Gardea-Torresdey, J. L. 2014. Organic-coated silver nanoparticles in biological and environmental conditions: Fate, stability and toxicity. *Adv. Colloid Interface Sci.* 204, 15–34.

Singh, N. P., Mc Coy, M. T., Tice, R. R., and Schneider, L. L. 1988. A simple technique for quantitation of low levels of DNA damage in individual cells. *Exp. Cell Res.* 175, 184–191.

Sussman, N. L., Gislason, G. T, Conlin, C. A., and Kelly, J. H. 1994. The hepatic extracorporeal liver assist device: initial clinical experience. *Artifical Organs*. 18, 390–396.

Tejamaya, M., Römer, I., Merrifield, R. C., Lead, J. R. 2012, Stability of Citrate, PVP, and PEG Coated Silver Nanoparticles in Ecotoxicology Media. *Environ. Sci. Technol*. 46, 7011−7017.

Tice, R. R., Agurell, E., Anderson, D., Burlinson, B., Hartmenn, A., Kobayashi, H., et al. 2000. Single cell gel / comet assay: guidelines for in vitro and in vivo genetic toxicology testing. *Environ. Mol. Mutagen.* 35, 206–221.

Toduka, Y., Toyooka, T., and Ibuki Y. 2012. Flow Cytometric Evaluation of Nanoparticles Using Side-Scattered Light and Reactive Oxygen Species-Mediated Fluorescence−Correlation with Genotoxicity. *Environ. Sci. Technol.* 46, 7629−7636.

Tomatis, M., Turci, F., Ceschino, R., Riganti, C., Gazzano, E., Martra, G., et al. 2010. High aspect ratio materials: Role of surface chemistry vs. length in the historical "long and short amosite asbestos fibers". *Inhal. Toxicol*. 22, 984–998.

Treuel, L., Brandholt, S., Maffre, P., Wiegele, S., Shang, L., and Nienhaus, G. U. 2014. Impact of protein modification on the protein corona on nanoparticles and nanoparticle-cell interactions. *ACS Nano.* 8, 503–513.

Verma A., and Stellacci F. 2010. Effect of surface properties on nanoparticle-cell interactions. *Small*. 6, 12–21.

Vinković Vrček, I., Pavičić, I., Crnković, T., Jurašin, D., Babič, M., Horák, D., et al. 2015. Does surface coating of metallic nanoparticles modulate their interference with in vitro assays? *RSC Adv.* 5, 70787–70807.

Vinković Vrček, I., Žuntar, I., Petlevski, R., Pavičić, I., Dutour Sikirić, M., Ćurlin, M., et al. 2016. Comparison of *in vitro* toxicity of silver ions and silver nanoparticles on human hepatoma cells. *Environ. Toxicol.* 31, 679–692.

Vranic, S., Boggetto, N., Contremoulins, V., Mornet, S., Reinhardt, N., Marano, F., Baeza-Squiban, A., Boland, S. 2013. Deciphering the mechanisms of cellular uptake of engineered nanoparticles by accurate evaluation of internalization using imaging flow cytometry. *Part. Fibre Toxicol.* 10:2. doi: 10.1186/1743-8977-10-2.

Wang, H., Wu, L., and Reinhard, B. M. 2012. Scavenger receptor mediated endocytosis of silver nanoparticles into J774A.1 macrophages is heterogeneous. *ACS Nano* 6, 7122–7132.

Zook, J. M., MacCuspie, R. I., Locascio, L. E., Halter, M. D., and Elliott, J. T. 2011. Stable nanoparticle aggregates/agglomerates of different sizes and the effect of their size on hemolytic cytotoxicity. *Nanotoxicology* 5, 517–530.

Zucker, R. M., and Daniel, K. M. 2012. Detection of TiO_2 nanoparticles in cells by flow cytometry. *Meth. Mol. Biol.* 906, 497–509.

Table 1. Size and dissolution behaviour of different silver nanoparticles (AgNP) in ultrapure water (UW) and cell-culture medium (CCM) supplemented with 10% (m/v) fetal bovine serum after 1 hr at 25 ^{o}C as measured by DLS, TEM and ICPMS. AgNP were functionalised with sodium bis(2-ethylhexyl)-sulfosuccinate (AOTAgNP), poly(vinylpyrrolidone) (PVPAgNP), bovine serum albumin (BSAAgNP), poly-*L*-lysine (PLLAgNP), and cetyltrimethylammonium bromide (CTABAgNP). TEM values indicate diameter size (*d* in nm) of AgNP, while DLS values indicated hydrodynamic diameter (d_H in nm) obtained from size distributions by volume. Dissolved Ag^+ fraction is given in % of total Ag content in AgNP suspensions.

NPs type	UW			CCM		
	d_H, nm (% mean volume)	*d*, nm (% total population)	Ag^+, %	d_H, nm (% mean volume)	*d*, nm (% total population)	Ag^+, %
AOTAgNP	19.9 ± 0.5 (99.4)	11.3 ± 0.6 (100)	0.21	47.8 ± 8.9 (99.7)	29.4 ± 1.4 (100)	1.17
PVPAgNP	4.9 ± 1.7 (98.7) 33.5 ± 4.0 (1.2)	3.8 ± 0.7 (76.5) 37.6 ± 5.2 (23.5)	2.72	59.6 ± 11.4 (99.8)	9.6 ± 1.7 (21.4) 29.8 ± 6.4 (78.6)	0.85
BSAAgNP	12.8 ± 8.1 (89.8) 65.7 ± 26.1 (8.7)	1.6 ± 0.4 (26.3) 8.7 ± 1.2 (73.7)	3.34	86.5 ± 17.5 (99.8)	18.4 ± 2.1 (100)	4.21
PLLAgNP	7.4 ± 1.3 (96.2) 55.7 ± 13.4 (3.7)	5.8 ± 0.9 (31.4) 21.7 ± 3.8 (68.6)	0.99	85.6 ± 17.6 (41.2) 208.4 ± 14.8 (56.7)	8.6 ± 1.6 (100)	0.72
CTABAgNP	17.4 ± 5.4 (88.1) 81.5 ± 7.6 (2.9) 193.6 ± 36.8 (8.7)	6.4 ± 1.2 (18.7) 21.9 ± 3.8 (22.5) 63.7 ± 12.4 (58.8)	0.44	71.8 ± 6.4 (98.9)	4.8 ± 0.7 (10.8) 27.8 ± 5.4 (72.6) 71.2 ± 15.1 (16.6)	1.14

Table 2. Evaluation of primary DNA damage in HepG2 cells following 24 hr exposure to silver nanoparticles functionalized with sodium bis(2-ethylhexyl)-sulfosuccinate (AOTAgNP), poly(vinylpyrrolidone) (PVPAgNP), bovine serum albumin (BSAAgNP), poly-*L*-lysine (PLLAgNP), and cetyltrimethylammonium bromide (CTABAgNP). Parameters of the alkaline comet assay were estimated on 110 comets per cell. Significant differences ($P < 0.05$) are denoted with * as compared to negative control.

Treatment		**Tail length**		**Tail intensity**	
		Mean ± SD	Median (range)	Mean ± SD	Median (range)
Negative control		17.20 ± 2.42	16.67 (13.33-24.58)	0.14 ± 0.41	0.03 (0-3.76)
Positive control		23.32 ± 3.78*	23.33 (15.83-33.33)	2.73 ± 4.21*	0.69 (0-27.08)
AOT AgNP	1 mg/L	17.96 ± 3.18	17.08 (13.33-30.00)	0.35 ± 1.01	0.05 (0-8.26)
	5 mg/L	21.56 ± 6.30*	19.17 (13.33-48.75)	2.15 ± 3.35*	0.70 (0-18.80)
	10 mg/L	32.48 ± 15.2*	27.08 (15.42-85.00)	4.12 ± 5.7*	1.85 (0-30.62)
PVP AgNP	1 mg/L	16.79 ± 1.61	16.25 (14.58-23.75)	1.21 ± 2.27*	0.14 (0-12.36)
	5 mg/L	21.08 ± 4.55*	19.58 (15.42-38.33)	1.57 ± 0.99*	0.15 (0-5.88)
	10 mg/L	25.56 ± 8.24*	24.17 (15-53.33)	2.31 ± 3.25*	0.92 (0-19.32)
BSA AgNP	1 mg/L	17.91 ± 2.49	17.08 (13.33-25.83)	0.22 ± 0.39	0.02 (0-2.01)
	5 mg/L	23.31 ± 7.06*	22.08 (14.58-59.58)	1.03 ± 1.55*	0.32 (0-6.92)
	10 mg/L	24.67 ± 5.52*	24.38 (16.25-47.50)	1.36 ± 1.71*	0.75 (0-8.10)
PLL AgNP	1 mg/L	16.44 ± 2.43	15.83 (12.08-25.83)	0.45 ± 0.76	0.10 (0-4.34)
	5 mg/L	19.86 ± 4.34*	17.08 (14.17-40.00)	0.84 ± 1.10*	0.34 (0-6.41)
	10 mg/L	46.53 ± 22.7*	40.00 (16.25-106.3)	11.64 ± 13.1*	7.54 (0.01-72.0)
CTAB AgNP	1 mg/L	17.79 ± 2.24	17.08 (14.17-25.83)	0.26 ± 0.50	0.04 (0-3.99)
	5 mg/L	19.82 ± 3.33*	18.75 (15.42-29.58)	0.23 ± 0.37	0.08 (0-3.50)
	10 mg/L	21.78 ± 5.76*	20.21 (14.17-59.58)	0.67 ± 1.97*	0.16 (0-22.16)

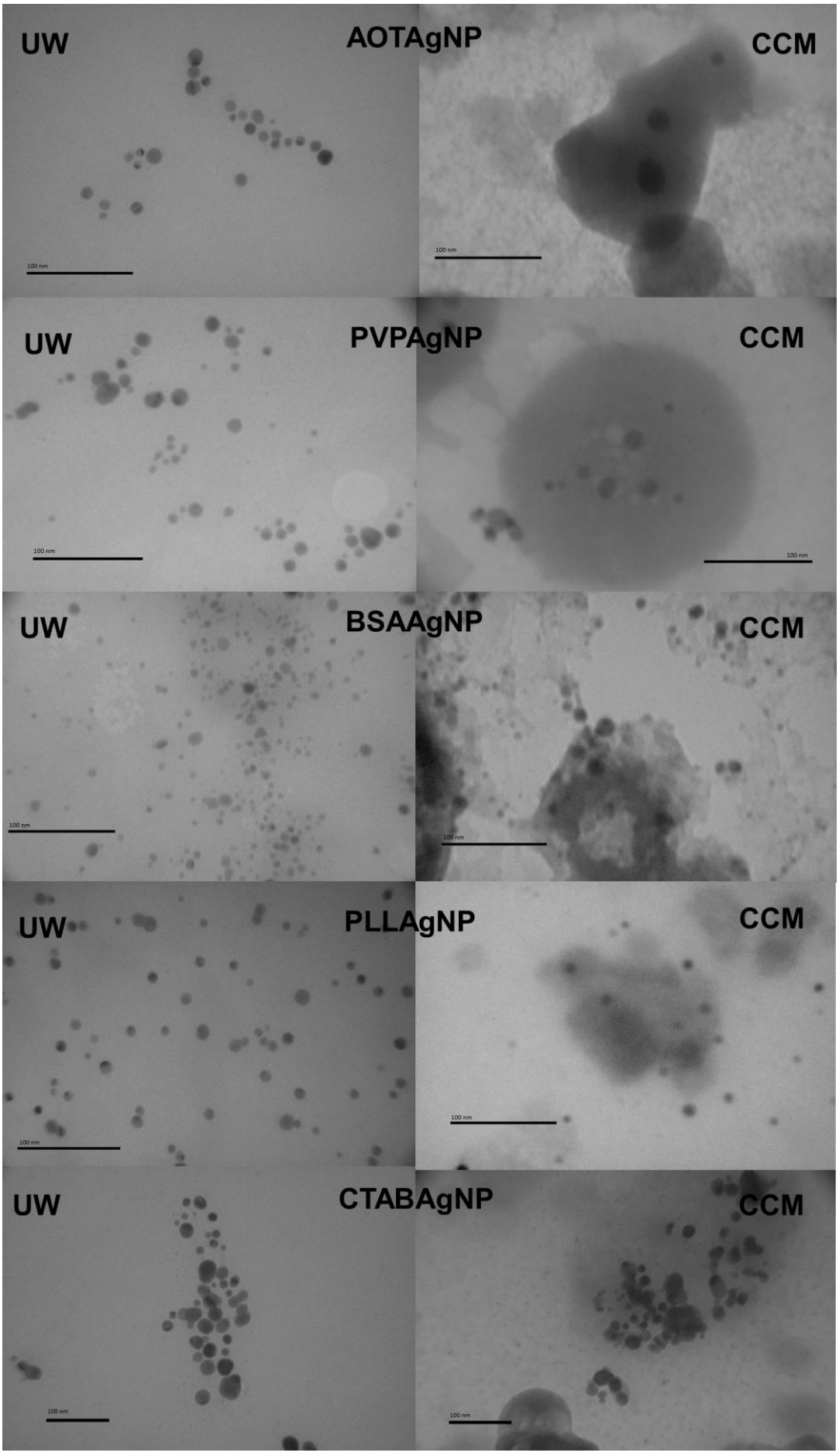
UW
AOTAgNP
CCM
100 nm
UW
PVPAgNP
CCM
100 nm
UW
BSAAgNP
CCM
100 nm
UW
PLLAgNP
CCM
100 nm
UW
CTABAgNP
CCM
100 nm

Fig. 1. Transmission electron micrographs (TEM) of different silver nanoparticles coated sodium bis(2-ethylhexyl)-sulfosuccinate (AOTAgNP), poly(vinylpyrrolidone) (PVPAgNP), bovine serum albumin (BSAAgNP), poly-*L*-lysine (PLLAgNP), and cetyl trimethylammonium bromide (CTABAgNP) in ultrapure water (UW) and cell-culture medium supplemented with 10% (m/v) fetal bovine serum albumin (CCM) after 1 hr at 25 ^{o}C. Scale bars are in 100 nm.

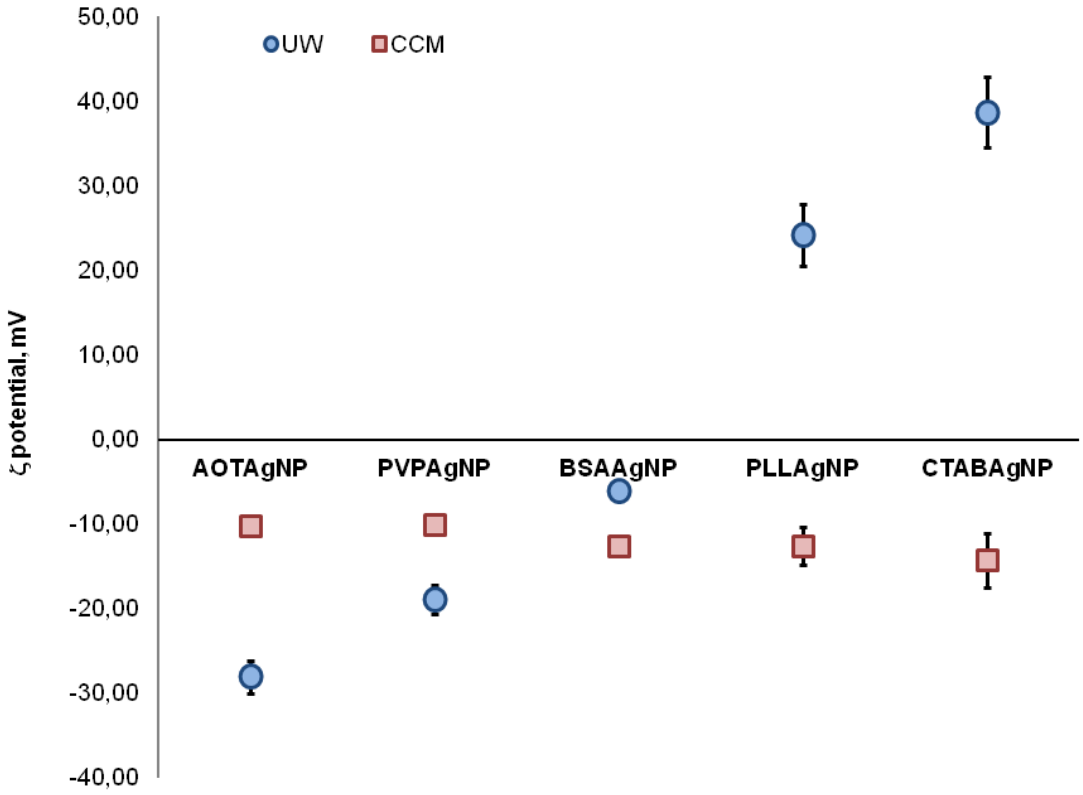

Fig. 2. Surface charge of different silver nanoparticles (AgNP) in ultrapure water (UW) and cell-culture medium supplemented with 10% (m/v) foetal bovine serum (CCM) after 1 hr at 25 ^{o}C as measured by ELS. AgNP were functionalised with sodium bis(2-ethylhexyl)-sulfosuccinate (AOTAgNP), poly(vinylpyrrolidone) (PVPAgNP), bovine serum albumin (BSAAgNP), poly-*L*-lysine (PLLAgNP), and cetyltrimethylammonium bromide (CTABAgNP).

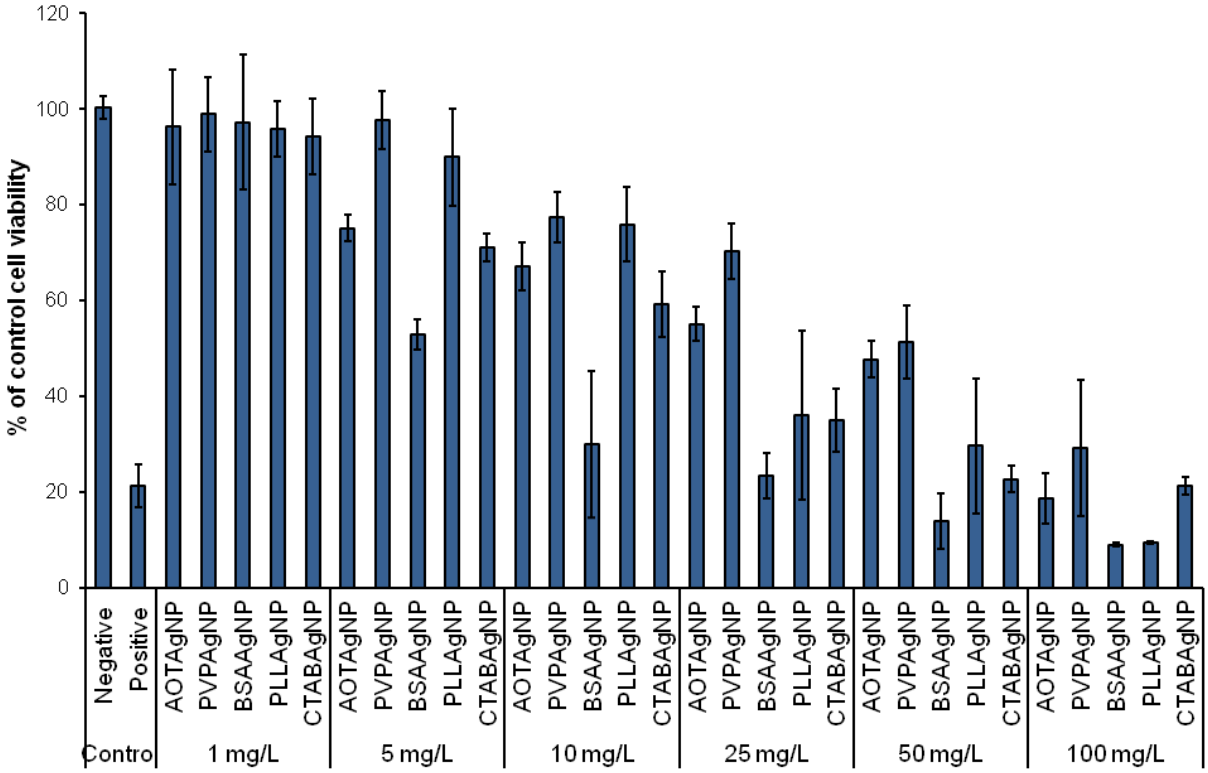

Fig. 3. Effect of different silver nanoparticles (AgNP) on the cell viability measured by the MTT assay. AgNP were functionalized with sodium bis(2-ethylhexyl)-sulfosuccinate (AOT), poly(vinylpyrrolidone) (PVP), bovine serum albumin (BSA), poly-*L*-lysine (PLL)**,** and cetyl trimethylammonium bromide (CTAB). HepG2 cells were exposed to different concentrations, given in mg/L, of AgNP for 24 hr. Control cells were cultivated in NPs-free exposure media (negative controls) or treated with DMSO (positive controls). The data for cell viability, expressed as the mean of three independent experiments conducted in five replicates, were calculated as percentages of the values measured in control cells. Error bars represent standard deviations.

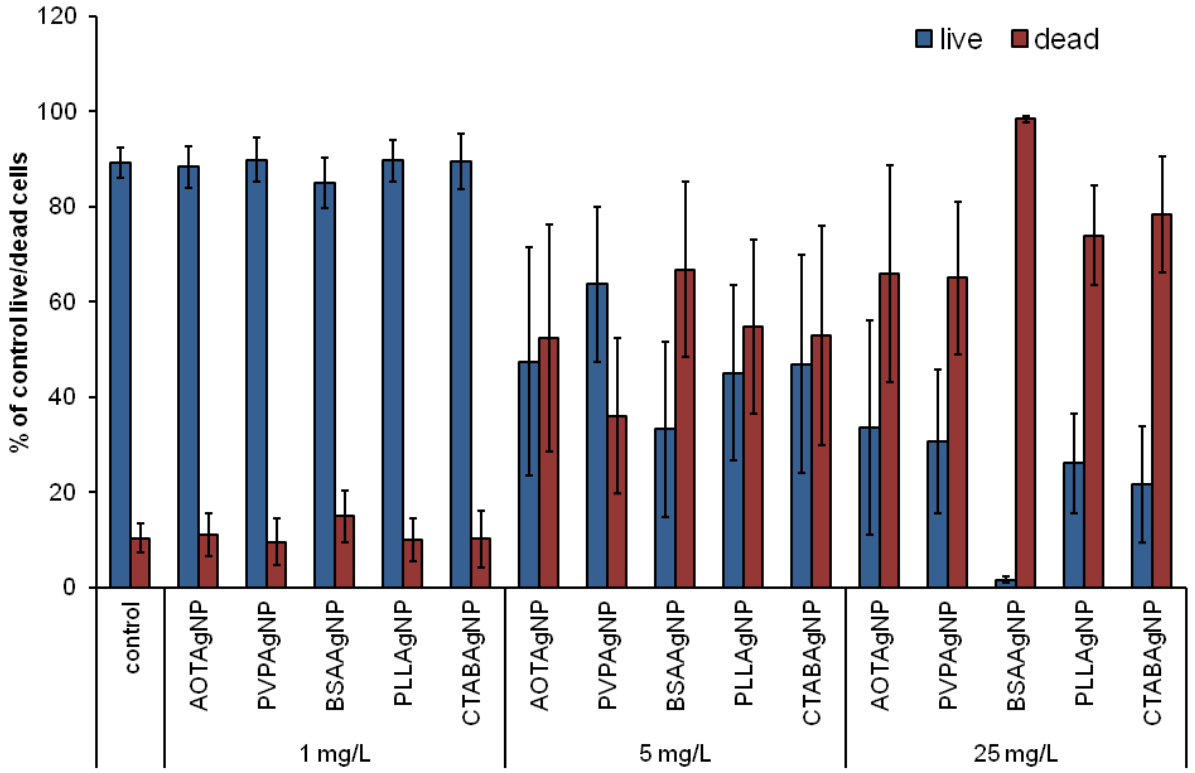

Fig. 4. Cell survival of HepG2 cells treated with different silver nanoparticles (AgNP) for 24 hr. AgNP were functionalized with sodium bis(2-ethylhexyl)-sulfosuccinate (AOT), poly(vinylpyrrolidone) (PVP), bovine serum albumin (BSA), poly-*L*-lysine (PLL)**,** and cetyl trimethylammonium bromide (CTAB). The percentage of live (EthD-negative, CAM-positive) and dead (EthD-positive, CAM-positive or negative) HepG2 cells was determined by the flow cytometry. Control cells were cultivated in NPs-free exposure media. Results, expressed as the mean of three independent experiments conducted in five replicates, were calculated as percentages of the values measured in control cells. Error bars represent standard deviations.

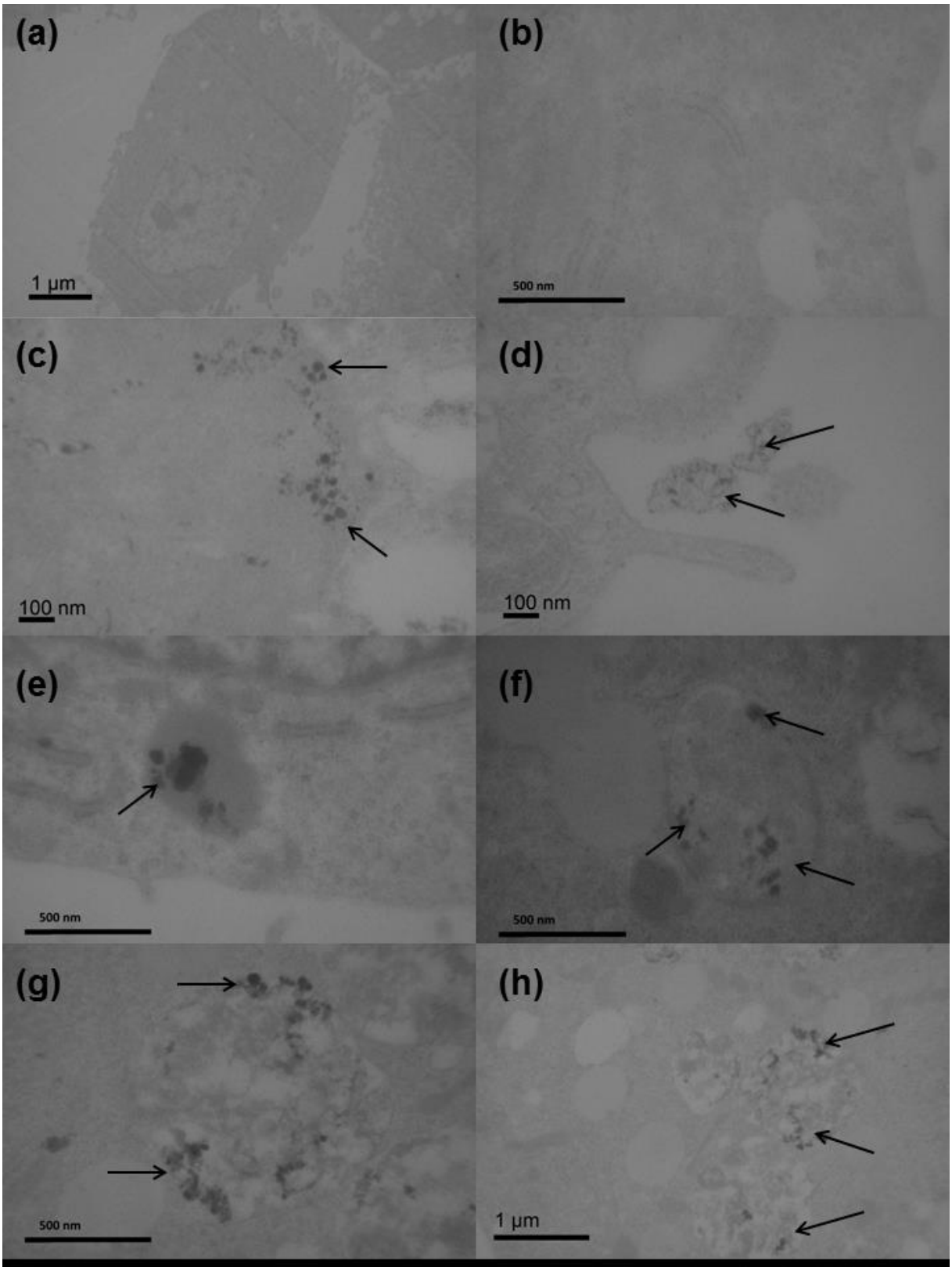

Fig. 5. Intracellular localization of different AgNP (indicated by blak arrows) in HepG2 cells investigated by TEM. (a, b) TEM images of untreated HepG2 cells with no morphological changes. (c) AOTAgNP found in large endosome after 24 hr exposure. (d) Process of

internalization of AOTAgNP in HepG2 cells. (e) Agglomerates of PVPAgNP found in membrane-bound structure. (f) BSAAgNP found in mitochondria of HepG2 cells. (g) Aggregates and single particles of PLLAgNP in lysosomes. (h) CTABAgNP found in lysosomes.

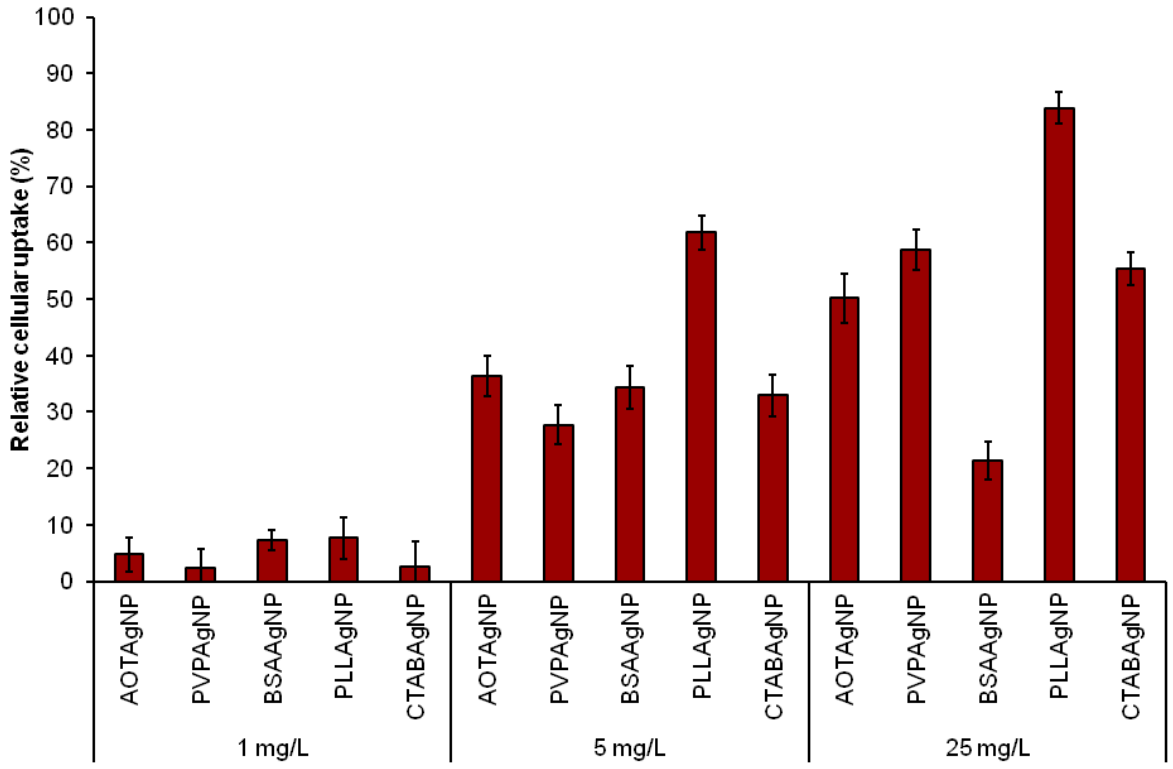

Fig. 6. Uptake of different silver nanoparticles (AgNP) by HepG2 cells analysed by the flow cytometry. AgNP were functionalized with sodium bis(2-ethylhexyl)-sulfosuccinate (AOT), poly(vinylpyrrolidone) (PVP), bovine serum albumin (BSA), poly-*L*-lysine (PLL)**,** and cetyltrimethylammonium bromide (CTAB). HepG2 cells were exposed to different concentrations of AgNPs, given in mg/L, for 24 hr. Control cells were cultivated in NPs-free exposure media (negative controls). The percentage of relative uptake, calculated as percentages of the increase of the side scattered light of the laser beam (SSC) relative to

control cells, is expressed as the mean of three independent experiments conducted in five replicates. Error bars represent standard deviations.

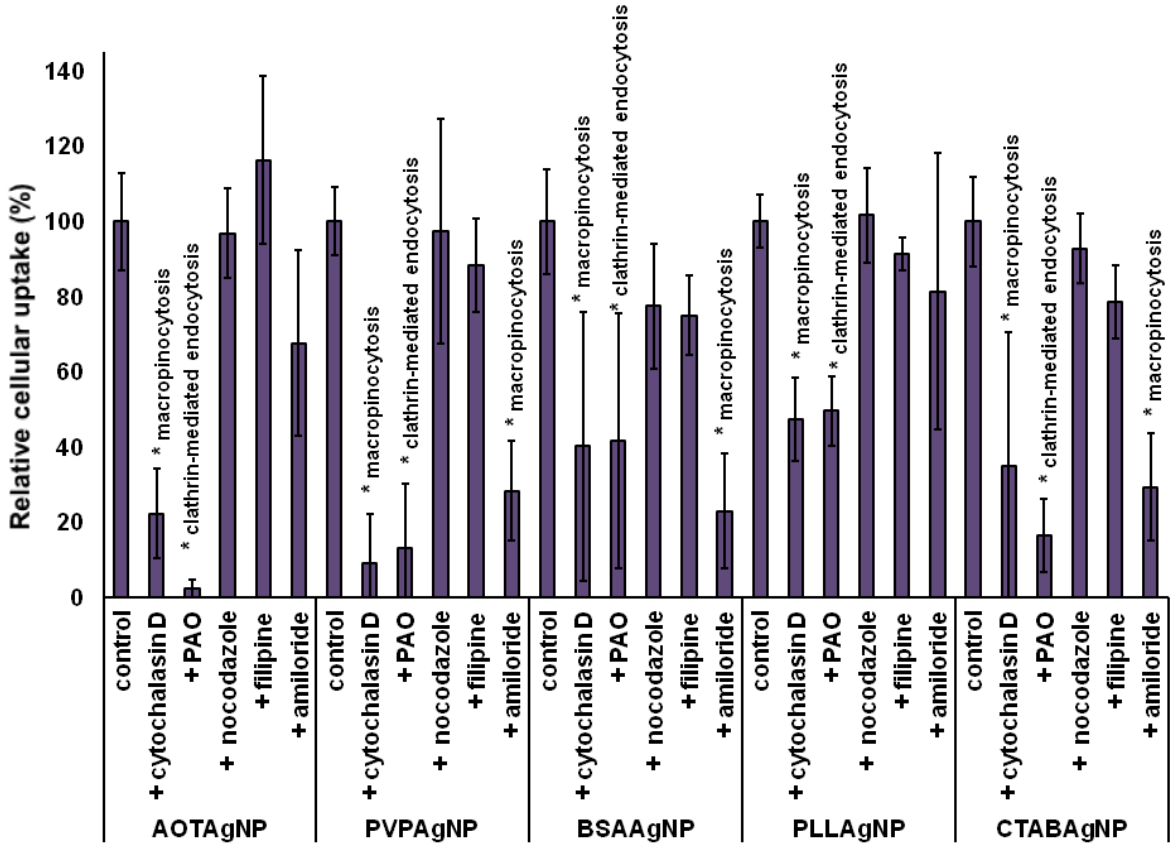

Fig. 7. Mechanism of uptake of different silver nanoparticles – functionalized with sodium bis(2-ethylhexyl)-sulfosuccinate (AOTAgNP), poly(vinylpyrrolidone) (PVPAgNP), bovine serum albumin (BSAAgNP), poly-*L*-lysine (PLLAgNP)**,** and cetyltrimethylammonium bromide (CTABAgNP) - by HepG2 cells analyzed by the flow cytometry. After treatment with different inhibitors: phenylarsine oxide (PAO), cytochalasin D, nocodazole, amiloride and filipin for 30 min, HepG2 cells were exposed to 5 mg/L AgNP for 4 hr. Control cells were cultivated in NPs-free exposure media (negative controls). The percentage of relative uptake, calculated as percentages of the increase of the side scattered light of the laser beam (SSC) relative to control cells, is expressed as the mean of three independent experiments conducted in five replicates. Error bars represent standard deviations.

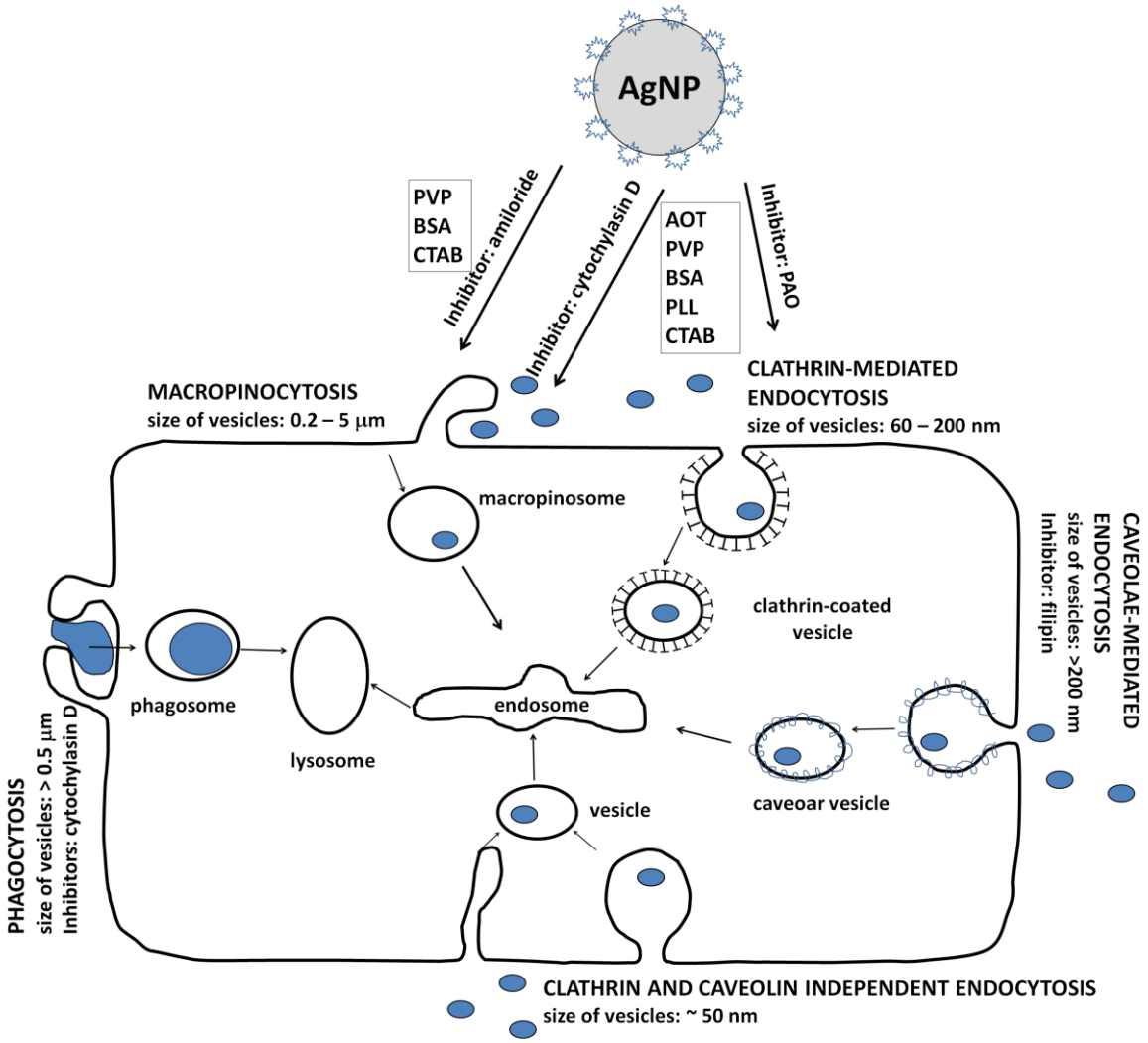

Fig. 8. Schematic presentation of endocytic pathways of different silver nanoparticles – functionalized with sodium bis(2-ethylhexyl)-sulfosuccinate (AOTAgNP), poly(vinylpyrrolidone) (PVPAgNP), bovine serum albumin (BSAAgNP), poly-*L*-lysine (PLLAgNP)**,** and cetyltrimethylammonium bromide (CTABAgNP) - in HepG2 cells.